Redox Biology 54 (2022) 102347

Contents lists available at ScienceDirect

Redox Biology

journal homepage: www.elsevier.com/locate/redox

The antioxidant enzyme Peroxiredoxin-1 controls stroke-associated microglia against acute ischemic stroke

Sinai Kim [a,1], Wonhyo Lee [b,1], Huiju Jo [a], Seong-Keun Sonn [a], Se-Jin Jeong [c], Seungwoon Seo [a], Joowon Suh [a], Jing Jin [a], Hyae Yon Kweon [a], Tae Kyeong Kim [a], Shin Hye Moon [a], Sejin Jeon [d], Jong Woo Kim [e,f], Yu Ri Kim [h], Eun-Woo Lee [e,f], Hwa Kyoung Shin [g], Sung Ho Park [b,**,1], Goo Taeg Oh [a,*,1]

[a] Heart-Immune-Brain Network Research Center, Department of Life Science, Ewha Womans University, Seoul, 03760, Republic of Korea
[b] Department of Biological Sciences, Ulsan National Institute of Science & Technology (UNIST), Ulsan, South Korea
[c] Cardiovascular Division, Department of Medicine, Washington University School of Medicine, St Louis, MO, USA
[d] Department of Biological Sciences and Biotechnology Major in Bio-Vaccine Engineering Andong National University, Andong, South Korea
[e] Metabolic Regulation Research Center, Korea Research Institute of Bioscience and Biotechnology (KRIBB), Daejeon, 34141, South Korea
[f] Department of Functional Genomics, University of Science and Technology (UST), Daejeon, South Korea
[g] Department of Korean Medical Science, School of Korean Medicine, Pusan National University, Yangsan, Gyeongnam, 50612, Republic of Korea
[h] KM Convergence Research Division, Korea Institute of Oriental Medicine 1672, Yuseong-daero, Yuseong-gu, Daejeon, 34054, Republic of Korea

ARTICLE INFO

Keywords:
Ischemic stroke
Stroke-associated microglia (SAM)
Reactive oxygen species (ROS)
Peroxiredoxin-1 (Prdx1)
Single cell RNA sequencing

ABSTRACT

Ischemic stroke is the leading cause of immortal disability and death worldwide. For treatment in the acute phase, it is necessary to control excessive reactive oxygen species (ROS) damage during ischemia/reperfusion (I/R). Microglia are well known to be closely associated with excessive ROS response in the early stage of I/R. However, the precise roles of microglia associated with mitigating ROS damage, and molecular markers of heterogenetic microglia in the I/R damaged brain has not been clarified. Here, we identified a new type of microglia associated with stroke in the I/R injured brain. Single-cell RNA sequencing (scRNA-seq) was used to assess transcriptional changes of microglia and immune cells in the contralateral (CL) and ipsilateral (IL) hemispheres after transient middle cerebral artery occlusion (tMCAO) surgery to mimic ischemic stroke. We classified a unique type of microglia with enhanced antioxidant function and markers similar to those of disease-associated microglia (DAM), designated them as stroke-associated microglia (SAM). The representative antioxidant enzyme, Peroxiredoxin-1 (Prdx1), was predominantly expressed in SAM and mediated ROS defense genes, including *Txn1, Srx1, Mt1,* and *Mt2*. In the *Prdx1*$^{-/-}$ I/R damaged brain, we observed significantly increased infarction, as assessed by TTC staining, and FACS analysis detected severe microglial cell death. Importantly, scRNA transcriptomics data showed that the SAM population was specifically decreased in *Prdx1*$^{-/-}$ mice and that these mice exhibited decreased ROS damage resistance. Inflammatory responses which were detected by ELISA and qPCR, were also increased in *Prdx1*$^{-/-}$ IL hemispheres. Finally, Prdx1-dependent antioxidative SAM were found to be essential for increasing the transcription levels of stroke-protective molecules, such as osteopontin and ferritin. A novel microglia type (SAM) is specifically activated in response to stroke I/R injury, and that Prdx1 expression is required for the activation and enhanced antioxidant function of SAM.

1. Introduction

Stroke is a significant cause of disability and death in adults worldwide. Of strokes, 80% present as sudden major cerebral artery occlusion resulting in ischemic damage and permanent neurological impairment [1]. Reactive oxygen species (ROS) have been implicated in brain damage after stroke reperfusion. Evidence shows that a rapid increase in ROS production immediately after acute ischemic stroke overwhelms antioxidant defenses, causing further tissue damage. In the infarct area,

* Corresponding author.
** Corresponding author.
E-mail addresses: parksu@unist.ac.kr (S.H. Park), gootaeg@ewha.ac.kr (G.T. Oh).
[1] These authors contributed equally to this study.

https://doi.org/10.1016/j.redox.2022.102347
Received 29 April 2022; Received in revised form 17 May 2022; Accepted 17 May 2022
Available online 25 May 2022

oxidative stress mediated by ROS promotes neurodegeneration and demyelination. While the mechanisms of stroke damage are complex, the associated brain damage is known to involve high levels of intracellular ROS [2]. Thus, it is critical to investigate antioxidant strategies that lead to the diminution of oxidative injury.

Abbreviations

tMCAO	transient middle cerebral artery occlusion
Prdx1	Peroxirodoxin-1
ROS	Reactive oxygen species
SAM	Stroke-associated microglia
DAM	Disease-associated microglia
IL	Ipsilateral
CL	Contralateral
I/R	Ischemia/reperfusion

Microglia, which are the principal resident immune cells in the brain, respond sensitively to ROS signaling [3]. Therefore, microglia are key actors in neuroinflammatory and neurodegenerative diseases [4–7]. Brain damage after stroke results in cell death, which activates resident glial cells and prompts peripheral immune cells to breach into the brain to perform various functions, including contradictory effects [8–10]. Recent studies reported that single-cell RNA sequencing (scRNA-seq) can be used to study the transcriptional heterogeneity of brain cells in neurodegenerative diseases and stroke [4–7,11–13]. The resident innate immune cells of the central nervous system (CNS) exert host defense functions, maintain normal tissue homeostasis, and support neuronal processes in the healthy brain [14–16]. Microglia are traditionally thought to comprise heterogeneous populations whose differences allow them to achieve a wide range of responses to environmental changes with the goal of maintaining CNS homeostasis [17]. Recent studies identified and examined a unique type of microglia associated with neurodegenerative diseases (DAM) that have the potential to restrict neurodegeneration, such as that seen in Alzheimer's disease (AD) [18–21]. However, the roles of heterogeneous microglia and their transformation to new populations have not been examined in detail in the stroke brain.

Peroxiredoxins (PRDXs) are a ROS-regulating enzymatic system in cells and tissues [22–24]. The PRDX family member, peroxiredoxin-1 (Prdx1), is a typical antioxidant enzyme that can reduce ROS stress and control the reduction-oxidation status of a cell under normal oxidative metabolism or oxidative stress [25–27]. Prdx1 is essential for regulating cell survival, inflammation, and oxidative stress in several CNS resident cell types, such as microglia, astrocytes, oligodendrocytes, and neuronal cells [28]. However, the function of Prdx1 in stroke is the subject of some debate. Several studies have revealed that Prdx1 protects against brain damage by reducing oxidative stress [29–33], while others found that Prdx1 contributes to enhancing brain damage as a damage-associated molecular pattern (DAMP) [34–36]. Therefore, we need to understand the intracellular and extracellular functions of the antioxidant enzyme, Prdx1, according to the damage severity and status of an ischemia-reperfusion (I/R) damaged brain.

In this study, we set out to identify a novel microglial subset that could protect against ROS-induced damage. We identify stroke-associated microglia (SAM), which exhibit an enhanced antioxidant defense that depends on Prdx1 expression and express markers similar to those of DAM. Finally, we show that *Prdx1* deficiency results in a specific decrease of the SAM population under the ischemic stroke, exacerbating I/R damage and death.

2. Materials and methods

2.1. Animal experiments

Mice were kept under specific pathogen-free (SPF) conditions with a 12 h light/dark cycle, 23 ± 1 °C, and 55 ± 10% humidity. All mouse experiments were approved by the Institutional Animal Care and Use Committee (IACUC N0. 21–054, 19-004) of Ewha Womans University and followed National Research Council Guidelines.

2.2. Mouse focal brain ischemia model

C57BL/6J male *Prdx1*$^{+/+}$ or *Prdx1*$^{-/-}$ mice, aged 8–9 weeks and weighing 20–24 g, were used for the focal brain ischemia experiments. *Prdx1*$^{-/-}$ mice were kindly provided by Dr. Dae-Yeul Yu at Korea Research Institute of Bioscience and Biotechnology (KRIBB) [37]. There was no significant difference in weight and age between the *Prdx1*$^{+/+}$ and *Prdx1*$^{-/-}$ mouse groups. All animals were randomized into different assays and the investigators were blinded to animal groups. We used a transient (60 min) middle cerebral artery occlusion (tMCAO) model induced through an intraluminal suture (Doccol, 701956PK5Re) under anesthesia with 1.5% isoflurane (SomnosuiteR, Kent Scientific). This tMCAO model was confirmed to reduce cerebral blood flow by 80–90%, as assessed by laser Doppler flowmetry (LDF, Primed 3000 system) to 10–20% of baseline blood flow. The rectal temperature was maintained at 37 ± 0.5 °C during surgery using a heating pad system. At 60 min after MCAO, the brain was reperfused by the withdrawal of the intraluminal suture. No mice have died during tMCAO surgery.

2.3. Brain cell isolation and preparation

Mice were anesthetized and subjected to cold PBS transcardial perfusion and each brain hemisphere was removed. The tissues were cut into pieces and transferred to gentleMACS™ C tubes (Miltenyi Biotec) containing the enzyme mixture provided with the Adult Brain Dissociation kit mouse and rat (Miltenyi Biotec, 130-107-677). The brain tissues were dissociated with the gentleMACS™ program 37 °C_ABDK_1, using 30 min incubations and a MACSmix tube rotator (Miltenyi Biotec). The supernatant was aspirated, and the pellet was resuspended in 8 ml of 40% Percoll (GE Healthcare, 17-0891-01) and overlaid on the top of 4 ml of 80% Percoll. The myelin debris was removed using Percoll separation. The gradient was centrifuged continuously at 2,200 rpm for 20 min at 22 °C. Single cells were collected from the 40%-to-80% interface, washed with PBS, and stained with a Zombie NIR™ Fixable viability kit (BioLegend, 423106). The isolated cells were washed twice with PBS.

2.4. Single-cell RNA sequencing and data processing

A BD FACS Aria III (BD Biosciences) was used for single-cell sorting of live brain cells from each brain hemisphere. Each cell suspension was subjected to 3′ single-cell RNA sequencing using a Single Cell A Chip Kit, a Single Cell 3′ Library and Gel Bead Kit V2, and an i7 Multiplex Kit (all from 10x Genomics) with a cell recovery target of 9000, following the manufacturer's instructions. Using the Cell Ranger toolkit (10x Genomics), libraries were sequenced on an Illumina HiSeq2500 and mapped to the GRCm38 (mm10) reference genome (v 2.1.0). The gene expression matrices generated by the Cell Ranger toolkit were analyzed on Seurat (v 4.0.2) [38]. Gene expression data from multiplet cells were identified by DoubletFinder (v 2.0.3) [39] using the developer's guidelines. Cells identified as multiplet were filtered, and in some cases (based on the intention of the analysis) only singlet data were merged. Additionally, Cd45 (Ptprc)-negative cells, cells with <200 detected genes, and cells with >20% of mitochondrial genes were filtered. The Seurat package's built-in function was used to visualize the dimension reduction plots, violin plots, heat map plots, and feature plots. In order to calculate statistical significance, p-values were calculated by the

Wilcoxon test using the ggpubr (v 0.4.0) package. Cell population plots and dot plots of differentially expressed genes were visualized by the ggplot2 package (v 3.3.5). The Wilcoxon test was used to calculate the p-values or differentially expressed genes, and the Holm method was used to calculate adjusted p-values for multiple comparison. $P < 0.05$ was considered significant, and p-values were indicated as $*P < 0.05$, $**P < 0.01$, and $***P < 0.001$. Enriched gene ontology was analyzed using the clusterProfiler package (v 3.18.1) [40], the GSE method, and the org.Mm.eg.db database package (v 3.12.0). The Seurat object was converted to a cell-data-set (CDS) by SeuratWrappers (v 0.3.0) to calculate pseudo-time order and predict trajectories among cells. Trajectories were calculated from CDS using the Monocle3 package (v 0.2.3.0) [41].

2.5. Infarction size measurement (2,3,5-triphenyltetrazolium chloride staining)

After 24 h of reperfusion, mice were sacrificed, and brains were quickly removed at 4 °C. Coronal slices (2mm) were made with a rodent brain matrix (Ted Pella, Inc.) and stained for 20 min at room temperature (RT) with 2% TTC (Sigma-Aldrich #T8877) solution in PBS. All infarct areas were positioned in the left hemisphere and the stained brain sections were chaptered on the same side. The infarct volume was calculated using the method of Swanson et al. (1990) [42] to compensate for brain swelling in the ischemic hemisphere. In brief, the sections were scanned, and the infarct area was calculated by subtracting the non-infarct area of the ipsilateral side from the area of the contralateral side using the ImageJ software (National Institutes of Health). Infarction area (%) = [Infarct area] / [Contralateral hemisphere area + Ipsilateral hemisphere area] X100. Infarct areas on each section were summed to give the total infarct area as 100%.

2.6. Neurological deficiency test

Neurological deficits were assessed by a neurological scoring system widely used in mice after tMCAO surgery [43]. The grading system was as follows: 0 = no deficit; 1 = forelimb weakness and torso turning to the ipsilateral side; 2 = circling to the affected side; 3 = unable to bear weight on the affected side; and 4 = no spontaneous locomotor activity or barrel rolling [44].

2.7. Rota-rod test

Motor coordination and balance were tested on a Rota-rod apparatus (Panlab S.L.U.). Before or after the tMCAO surgery, *Prdx1*$^{+/+}$ or *Prdx1*$^{-/-}$ mice were tested on Rota-rod consisting of five trials for each. The rod was rotated at 18 rpm and the latency to falling off was recorded and averaged.

2.8. Ultrasound assessment of cerebral carotid artery

Prdx1$^{+/+}$ or *Prdx1*$^{-/-}$ mice were used for the assessment of blood flow and vessel function at the cerebral carotid artery (CCA). VisualSonics Vevo 2100 machine was specifically designed for mice and used to perform CCA ultrasound. Mice were anesthetized with 1% isoflurane and oxygen during the echo procedure. Aortic arches and CCA were viewed and analyzed in B-mode, and PW-mode. CCA diameter, and cardiac flow velocities of CCA were measured offline (Vevo software).

2.9. Nissl staining

Nissl (Sigma-Aldrich, C0775) staining was used to detect brain cells from normal brains of *Prdx1*$^{+/+}$ and *Prdx1*$^{-/-}$ mice before the tMCAO surgery according to the manufacturer's instructions. All experiments were repeated three times.

2.10. Evans blue and microfil injection staining

Prdx1$^{+/+}$ or *Prdx1*$^{-/-}$ mice were used for the assessment of blood flow and vessel function at the cerebral carotid artery (CCA) and internal carotid artery (ICA). 2% Evans blue (100μl per mice) was intravenously injected into mice before and after tMCAO surgery. For the Microfil injection staining, mice were anesthetized and subjected to warm PBS transcardial perfusion and injected with microfil solution for 12 h at 4 °C. Brain samples were taken after the decalcification of the skull.

2.11. Bone marrow transplantation (BMT)

Prdx1$^{+/+}$ and *Prdx1*$^{-/-}$ donor mouse femurs and tibia were dissected. PB buffer (0.5% BSA in PBS) was used to flush the marrow from each bone. MACS LD columns (Miltenyi Biotec) were used to deplete mature T cells from the BM cells. Four-week-old *Prdx1*$^{+/+}$ and *Prdx1*$^{-/-}$ recipient mice were lethally irradiated using gamma rays (5Gy X 2, 4 h intermission) and 1.0×10^6 BM cells suspended in 100 μl of PBS were administered intravenously to the irradiated recipient mice. Each mouse in a silicone-capped tube was irradiated individually to prevent other brain damage. At 4 weeks after BM transplantation, the mice were used for tMCAO surgery.

2.12. Flow cytometric analysis

Single cells were incubated with monoclonal anti-CD16/32 (BioLegend, 101302) at 4 °C for 30 min in FACS buffer (DPBS containing 2% FBS) to block the Fc receptors. The cells were then stained with anti-CD45/APC (BioLegend, 103124), anti-CD11b/BV510 (BioLegend, 101263), anti-Ly6G-FITC (BioLegend, 108417), anti-Ly6c-BV421 (BioLegend, 128014), anti-CD11c-PE/cy7 (BioLegend, 117318), anti-MHCII-APC/cy7 (BioLegend, 107628), anti-CD206-PE (BioLegend, 141732), anti-CD63-PE/cy7 (Biolegend, 143910), anti-Spp1-PE (R&D, IC808P), and anti-Fth1-FITC (biobyt, orb102585) in FACS buffer at 4 °C for 30 min, and washed twice with FACS buffer. Intracellular ROS levels were detected by H_2DCFDA (Invitrogen, C6827) and Bodipy 493/503 (Invitrogen, D3922) staining. To determine the apoptosis of microglia, flow cytometry analyses were performed using Annexin V-APC apoptosis detection kits (BD, 556547). All antibodies were used at the concentrations recommended by the manufacturer. After being filtered through a round-bottom tube with a 70 μm strainer cap, the cells were analyzed using a BD LSRFortessa™ Cell Analyzer and the FlowJo v10 software (both from BD Biosciences in Fluorescence Core Imaging Center of Ewha Womans University).

2.13. Quantitative real time-PCR analysis (qPCR)

Total RNA was isolated from brain tissues of tMCAO mice using the TRIzol Reagent (Life Technologies) and diluted in diethylpyrocarbonate (DEPC; Sigma-Aldrich)-treated water. cDNA was synthesized using a Revert Aid First Strand cDNA Synthesis Kit (Thermo Fisher Scientific, K1622). qRT-PCR was performed using an ABI PRISM 7300 sequence detection system (Applied Biosystems) and the SYBR green PCR master mix (KAPA Biosystems, KK4602) according to the manufacturers' specifications. Reactions were performed in duplicate using 20 μg cDNA as template, 10 pM forward and reverse primers, and the reagents of a StepOnePlus Real-Time PCR System (Applied Biosystems). The circulation was performed using the comparative method ($-2^{\Delta CT}$) that the cycle number at which the transcripts of the gene of interest were detectable CT was normalized to the cycle number of β-actin detection. The fold change of the gene of interest relative to the control was expressed as $2^{-}_{\Delta\Delta CT}$.

2.14. BV-2 cell transfection and oxygen glucose deprivation/reperfusion (OGD/R)

BV-2 cells were transfected with 40 μM siRNA utilizing a Neon® Transfection System (Invitrogen, MPK1096) and used at 48 h post-transfection. Negative control siRNA (siCTL) and siRNA against mouse *Prdx1* (si*Prdx1*) were purchased from Bioneer (Korea). For OGD/R, BV-2 cells were seeded in 12-well cell culture plates at 3.0×10^5 per well and incubated with complete DMEM (HyClone SH302437.01) in a normoxic incubator with 5% CO_2 at 37 °C for 24 h. For OGD treatment, cells were incubated with 1% dFBS (Gibco, 26400044) in DMEM (Gibco, A14430-01) under an acidotic condition (Sigma-Aldrich, L426) for 5 h at 37 °C in an anaerobic incubator with 95% N_2 and 5% CO_2. For R treatment, the culture medium was replaced with complete DMEM, and the cells were cultured for 24 h in a normoxic incubator with 5% CO_2 at 37 °C. For ferroptosis inhibition in BV-2 cells, 2 μM ferrostatin-1 (Selleckchem, S7243) was applied to 1.5×10^5 cells per well in a 24-well plate, and the cells were incubated in 5% CO_2 at 37 °C for 24 h. After OGD/R treatment, the cell viability of BV-2 cells was detected using Cell titer Glo 2.0 (Promega, G9243) and crystal violet staining (Sigma-Aldrich, C0775) according to the manufacturer's instructions. All experiments were repeated three times.

2.15. Primary microglia cell protein prep assay

Microglia were sorted from tMCAO surgery mouse brains using microglia MicroBeads (Miltenyi Biotec, 130,093,634) according to the manufacturer's instructions, and lysed with LIPA buffer (1% Triton X-100, 0.1% SDS, 2 mM EDTA) with a protease inhibitor cocktail (Roche Life Science, 11,697,498 001). Protein samples were stored at −80 °C.

2.16. Western blot analysis

For Western blot analysis, proteins were electrophoresed in 10% sodium dodecyl sulfate-polyacrylamide gels and transferred to polyvinylidene fluoride membranes using standard electroblotting procedures. The membranes were blocked with 4% skim milk in TBST (TBS; 50 mM Tris-Cl, 150 mM NaCl, pH 7.5) containing 0.5% Tween 20 and immunolabeled overnight at 4 °C with primary antibodies against osteopontin (Abcam, ab63856), β-actin (Santa Cruz, sc47778), or GAPDH (GeneTex, GTX-100118). The appropriate HRP-conjugated secondary antibodies were applied (EMD Millipore) and immunolabeling was detected by an enhanced chemiluminescence kit (Westsave, LF-QC0101).

2.17. ELISA

Blood samples were obtained from tMCAO model mice anesthetized with 2.4% Avertin (10 μl/g). Serum samples were isolated by centrifugation (4 °C, 15 min, 1500 rpm), collated as the supernatant, and stored at −80 °C. ELISA was performed using commercially available kits for ELISA of Il-1β, Il-6, and Ccl-2 (R&D Systems, DY401, DY406, DY479).

2.18. Immunofluorescence staining

Mice were euthanized and transcardially perfused with PBS and 4% paraformaldehyde (Sigma-Aldrich) in PBS, and brains were harvested and cryoprotected in 15% and 30% sucrose in PBS overnight each day. Each brain was embedded in 100% OCT compound (Leica), frozen at −80 °C, and sectioned at 20 μm. Sections were attached to slides overnight, blocked with blocking solution (5% BSA, and 0.5% Triton X-100 in PBS) for 1 h, incubated with the primary antibody at 4 °C overnight, and incubated with an Alexa 488-conjugated secondary antibody (Life Technology) for 3 h at room temperature. The following primary antibodies and dilutions were used: anti-IBA-1 (Wako, 019–19741, Novous,10028s), Fth1 (Lifespan, LSB5847), Cd63 (Novous, 10077813), Spp1 (Novous, 110–89062) and, anti-c-Caspase-3 (Cell Signaling, 9661). The average number of c-caspase-3 positive cells in five random fields of interest at the damaged brain was evaluated in each animal. Slides were counterstained with 4',6-diamidino-2-phenylindole (DAPI), and images were obtained using a confocal microscope (Carl Zeiss; LSM 780, LSM 880 in Fluorescence Core Imaging Center of Ewha Womans University).

2.19. TUNEL assay and crystal violet staining

TUNEL assay and crystal violet staining were used to detect apoptotic cell death in I/R injured brains. TUNEL assay was performed using a TUNEL Assay kit-HRP-DAB (Abcam, ab206386) according to the manufacturer's instructions. Crystal violet (Sigma-Aldrich) staining was used to detect enlarged areas of stroke damage according to the manufacturer's instructions. Stained cells were detected with the ImageJ software.

2.20. Statistical analysis

Statistical analyses were performed using GraphPad Prism 8 software. All results are expressed as the means ± S.E.M from at least three independent experiments. For animal experiments, the statistical significances of differences were determined by the two-tailed unpaired Student's t-test on normally distributed continuous data. More than 2 groups were subjected to 2-way ANOVA with Turkey's multiple comparison test. $P < 0.05$ was considered statistically significant. The mouse Kaplan-Meier survival rate was measured by the number of deaths 24 h reperfusion after tMCAO surgery and tested by the Gehan-Breslow-Wilcoxon test.

2.21. Data availability

Data for this project have been deposited at NCBI's Gene Expression Omnibus (GEO) and GSE number is GSE197731. (https://www.ncbi.nlm.nih.gov/geo/query/acc.cgi?acc=GSE197731).

3. Results

3.1. Single-cell transcriptomic heterogeneity of immune cells in the stroke brain

Most of the previous studies on the immune cells involved in ischemic stroke were based on immune cell populations sorted using a small set of cell-surface markers. These approaches were limited in their ability to shed light on the heterogeneity of immune cells and the existence of additional immune cell types, and were not suitable for tracking dynamic gene expression in immune subsets according to stroke progression. Recent studies have demonstrated that single-cell analysis of brain cells in neurodegenerative diseases, such as AD and amyotrophic lateral sclerosis (ALS), is a highly valuable tool for defining the heterogeneity of brain cells and identifying additional cell types [4,18,45–48]. Thus, to characterize the immune cell types and states involved in I/R stoke injury, we herein induced ischemic stroke by transient middle cerebral artery occlusion (tMCAO) surgery in male C57BL6/J mice, and isolated ipsilateral (IL) and contralateral (CL) hemispheres after 24 h and 48 h of reperfusion post-tMCAO (Fig. 1A, n = 3 for each group). All cells from each brain hemisphere were labeled with a viability dye and sorted simultaneously (Supplementary Fig. S1A). scRNA-seq analysis was used to characterize the heterogeneous transcriptomic responses of resident and infiltrated immune cells during acute ischemic stroke. Unbiased clustering of all 19,488 single cells sorted from the IL and CL hemispheres after 24 h and 48 h of reperfusion post-surgery was used to generate a detailed map of six transcriptionally distinct subpopulations (Fig. 1B). Clusters corresponding to macrophages/monocytes (*Cd68, Adgre1*), granulocytes (*Cxcr2*), lymphoid cells (*Cd3d*), proliferating cells (*Ki67*$^+$), and microglia (*Tmem119, Cx3cr1,*

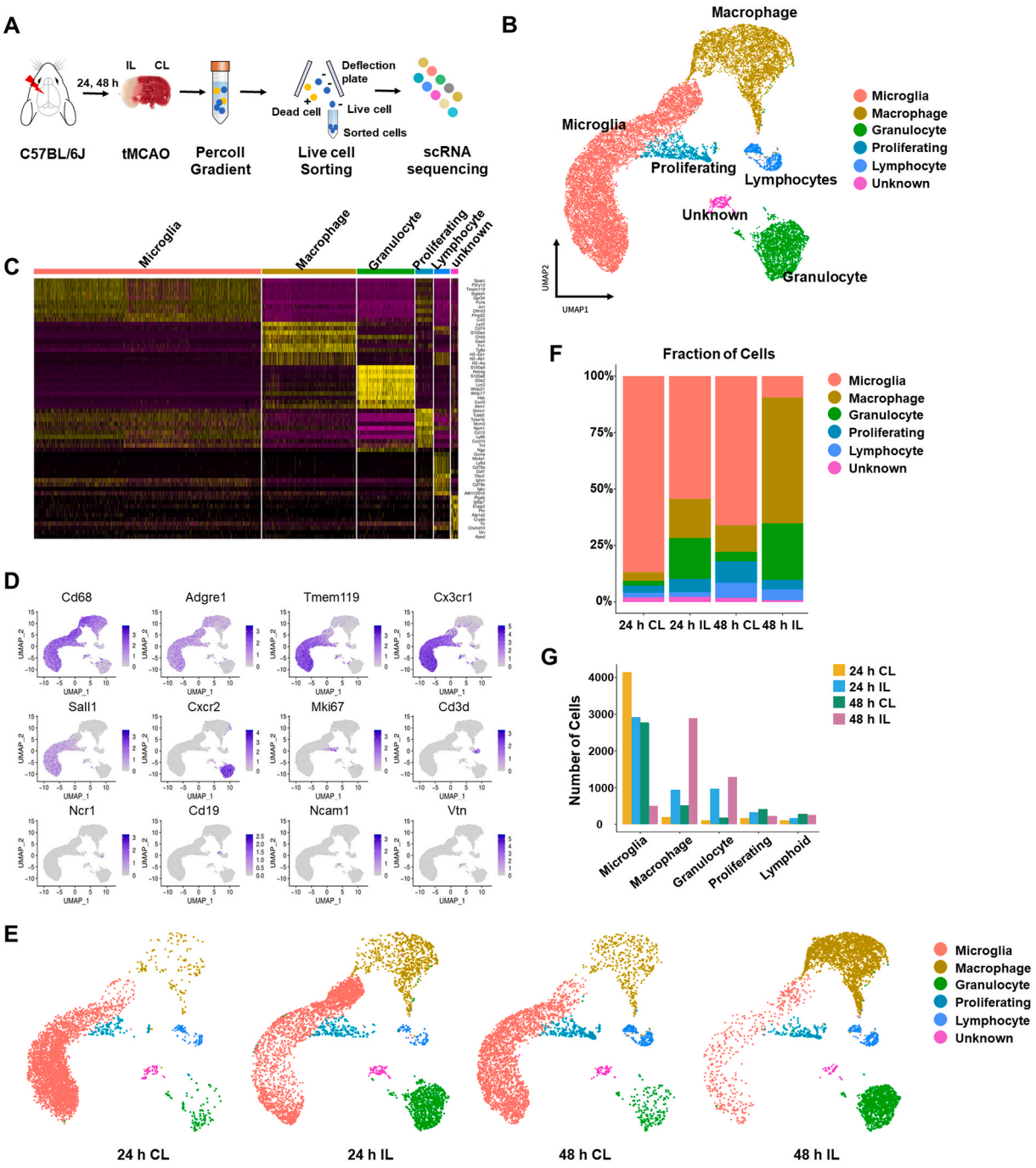

Fig. 1. scRNA-seq reveals heterogeneity of immune cells in the stroke brain. (A) Experimental design for scRNA-seq (n = 3 per group). Cells in each group were pooled up to 9000 target cells per hemisphere. **(B)** UMAP plots showing clusters and annotations of cells identified in stroke brains obtained at 24 h and 48 h after tMCAO. **(C)** Heatmap showing the relative expression levels of the top marker genes in the six cell types identified by scRNA-seq. **(D)** UMAP plots showing representative markers for each cell cluster in the ischemic brain. **(E)** UMAP plot showing clusters of each hemisphere cell population at 24 h and 48 h after tMCAO. **(F)** Stacked bar graphs showing the proportion of cells identified in each cluster out of the total number of cells at 24 h and 48 h after tMCAO. **(G)** Bar graphs showing total cell numbers identified in clusters of each hemisphere at 24 h and 48 h after tMCAO.

Sall1) were clearly distinguished (Fig. 1C and D, Supplementary Fig. S1B). Also, UMAP plots from IL and CL hemispheres at 24 h and 48 h showed that the distributions of microglia and immune cells changed dynamically with the level of ischemic damage over time (Fig. 1E). Comparison between the IL and CL hemispheres revealed that the proportion of microglia in the IL hemisphere at 24 h was significantly decreased by ischemic damage, while those of infiltrating macrophages and granulocytes were increased (Fig. 1E–G). Interestingly, microglia were differently distributed in the IL hemisphere compared to the CL hemisphere, implying that acute ischemic damage caused heterogeneity in the population of microglia (also discussed below). At 48 h after surgery, the microglia were greatly reduced and infiltrated cells such as macrophages and granulocytes held a majority in the IL hemisphere (Fig. 1E–G). A small number of lymphocytes were also observed; however, their level changed minimally between 24 h and 48 h, consistent with previous studies showing that innate immune cells first arrive 1–2 days after tMCAO surgery [49,50]. We observed more infiltrated immune cells in the CL hemisphere at 48 h than at 24 h, suggesting that the

effect of ischemic damage spreads to the CL hemisphere over time (Fig. 1E–G). Classical FACS analysis using well-known markers (Supplementary Fig. S1C) confirmed that resident microglia were decreased with time and infiltrated immune cells, including macrophages, were increased in the IL hemisphere to a maximal level at 48 h post-stroke in mice (Supplementary Figs. S1C and D). Overall, our scRNA-seq analysis of transcriptional levels in tMCAO model mice provides information on distinct cell populations that protect against acute stroke I/R damage and defines heterogeneous cell populations in both IL and CL hemispheres.

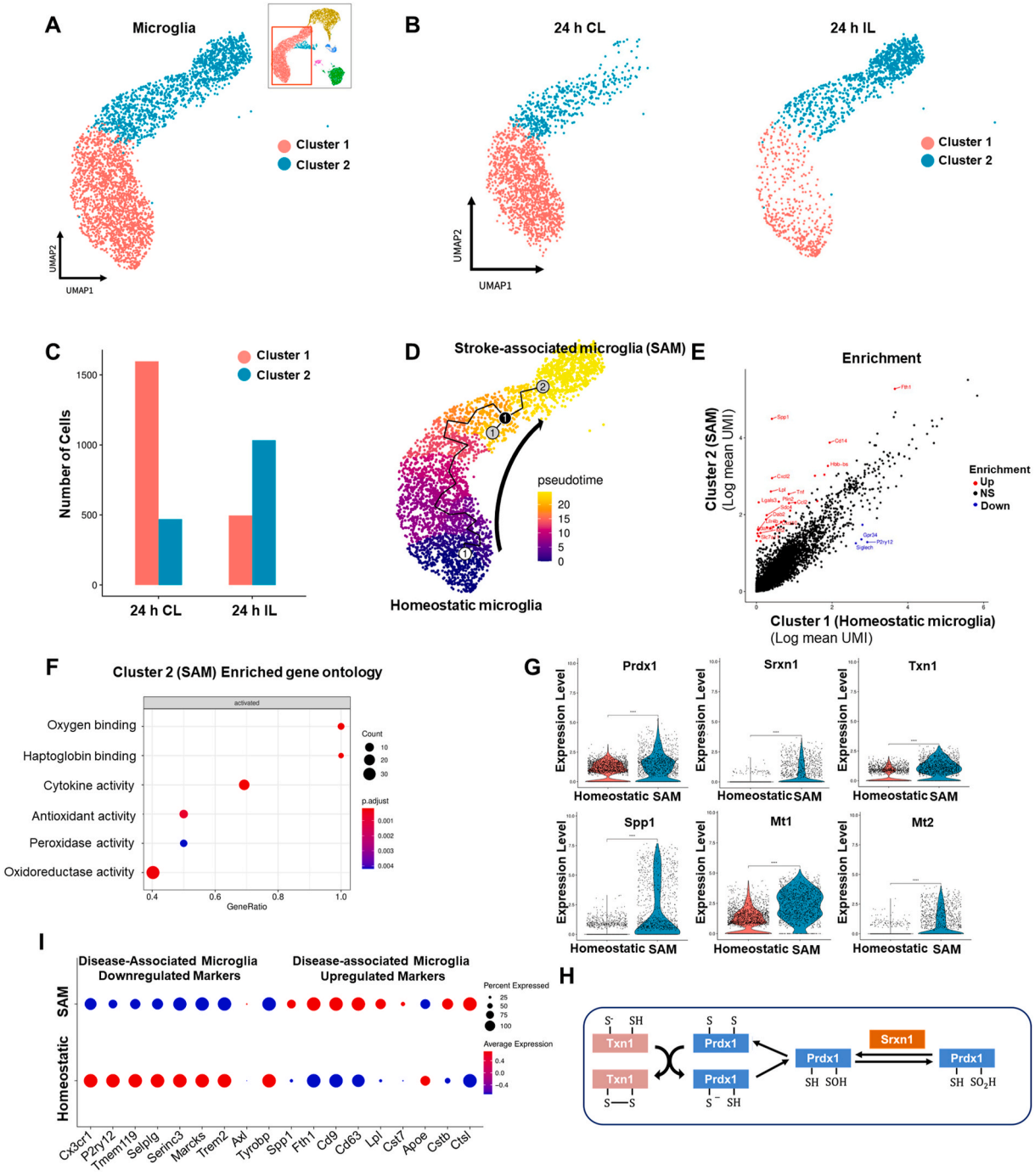

Fig. 2. Stroke-associated microglia (SAM) exhibit enhanced antioxidant properties. (A) Subclustering analysis of microglia in the stroke brain. Microglia (10,559 cells) were extracted from CL and IL hemispheres at 24 h and 48 h after tMCAO. **(B)** UMAP plots showing two microglia clusters from CL (left) and IL (right) hemispheres at 24 h after tMCAO. **(C)** Stacked bar graph showing numbers of microglia counted from IL and CL hemispheres at 24 h after tMCAO. **(D)** Projection of microglia on a pseudo-time graph plot displaying the transition from homeostatic microglia (blue) to SAM (yellow). **(E)** Scatterplot showing scRNA-seq analysis of differentially expressed genes. Red and blue dots indicate genes that were significantly increased and decreased, respectively, in SAM (log2FC>±1.5). **(F)** Gene ontology analysis of genes found to be differentially expressed in SAM. **(G)** Violin plots showing the expression of the SAM marker genes, *Prdx1, Srxn1, Txn1, Spp1, Mt1*, and *Mt2* in microglial subclusters. **(H)** Prdx1-mediated antioxidant pathways against ROS stress. **(I)** Expression of DAM marker genes in SAM and homeostatic microglia. Red and blue lines respectively indicate up- and down-regulated marker genes of DAM. Increased or decreased gene expression in SAM versus homeostatic microglia is indicated by red or blue dots, respectively. . (For interpretation of the references to colour in this figure legend, the reader is referred to the Web version of this article.)

3.2. Identification of a unique stroke-associated type of microglia

Differential gene expression (DEG) analysis between IL and CL hemispheres using all microglia obtained at the 24 h timepoint revealed that stroke I/R damage caused transcriptional reprogramming in the IL hemisphere: We observed up-regulation of a wide range of genes, including *Spp1, Fth1,* and *Cxcl2,* and down-regulation of some heat shock protein-encoding genes (Supplementary Figs. S2A and B). To investigate microglial heterogeneity associated with stroke I/R damage, we performed subclustering analysis with microglial data (10,599 cells) obtained from the IL and CL hemispheres at 24 h after tMCAO. Microglia were separated into two distinct clusters based on their gene expression patterns (Fig. 2A). As expected, the total cell number of microglia in the IL hemisphere was highly decreased by acute I/R damage. However, subclustering analysis of microglia showed that the two distinct clusters had different responses to stroke I/R damage in the two hemispheres (Fig. 2B). In the homeostatic CL hemisphere, cluster 1 represented a dominant population of microglia while cluster 2 consisted of relatively few cells. In the IL hemisphere subjected to ischemic damage, in contrast, the number of cluster 2 microglia were significantly increased, whereas the total number of microglia and the number of cluster 1 cells were decreased (Fig. 2C). These data suggest that cells of cluster 2 are a unique microglial population associated with stroke injury and may potentially play a protective role against ischemic wounds. Consistently, pseudo-time trajectory analysis (Fig. 2D) demonstrated that there was a temporal transcriptomic alteration from cluster 1 to cluster 2, indicating that there is transcriptomic continuity between the two clusters and the microglial transcriptomic pattern is shifted from cluster 1 to cluster 2. Thus, we annotated the cluster 1 and cluster 2 microglia as homeostatic microglia and stroke-associated microglia (SAM), respectively. To gain insight into the gene regulation of SAM and determine the signature phenotype, we performed DEG analysis and gene ontology (GO) analysis (Fig. 2E and F). The gene expression pattern of SAM showed a regulatory pattern distinct from that of homeostatic microglia. GO analysis of DEG revealed that the genes up-regulated in SAM corresponded to anti-oxidative and oxygen-binding pathways related to ischemic injury phenotypes, as well as pathways that have inflammatory properties. In line with our findings of enhanced peroxidase and oxidoreductase activity, the expression levels of peroxiredoxin-1 (*Prdx1*), sulfiredoxin-1 (*Srxn1*), thioredoxin-1 (*Txn1*), and metallothionein-1, 2 (*Mt1, 2*) were significantly increased in SAM (Fig. 2G). These data suggest that SAM represent a specialized and distinctive type of microglia that regulates the Prdx1-Srxn1-Txn1 system [51,52] (Fig. 2H) to defend against oxidative stress.

Previous reports revealed that a new type of microglia associated with AD and ALS contributes to restricting neurodegeneration [18]. These disease-associated microglia (DAM) explained the cellular heterogeneity and the roles of immune cell subsets in these neurodegenerative diseases. Thus, we herein compared the gene expression and known markers of DAM with those of our novel SAM population (Fig. 2I). We found that the markers commonly downregulated in DAM, including *Cx3cr1, P2ry12, Tmem119, Selplg, Serinc3*, and *Marcks*, were downregulated in SAM while the markers upregulated in DAM, such as *Spp1, Fth1, Cd9, Cd63, Lpl, Cst7, Cstb,* and *Ctsl,* were upregulated in SAM. This similarity indicates that SAM may be a kind of DAM that responds to brain pathology. However, we did not observe any enrichment of oxidative stress-related genes in DAM, suggesting that SAM represent a unique population of microglia that is induced by stroke and limits oxidative stress by reducing ROS in the tMCAO model. To our knowledge, this is the first report to show stroke-induced heterogeneity of microglia and identify SAM as a unique population of microglia that play potential antioxidant roles in stroke.

3.3. Prdx1 depletion exacerbates ischemic brain injury and microglial cell death

Previous studies provided substantial evidence that oxidative stress and ROS are the key deleterious factors in the pathophysiology of stroke I/R, and endogenous antioxidant protection restricts the harmful effects of oxidative stress [2,53]. To address whether antioxidant molecules are required for antioxidant defenses and the development of SAM, we assessed the *in vivo* phenotype of *Prdx1*$^{-/-}$ mice in the tMCAO model. Prdx1 is a peroxiredoxin family member that plays an important role in protecting cells against oxidative stress by detoxifying peroxides. In *Prdx1*$^{+/+}$ and *Prdx1*$^{-/-}$ mouse brains, the total infarction volume at 24 h following tMCAO surgery was calculated by summing the infarction volumes measured in each slice after TTC (2,3,5-triphenyl tetrazolium chloride) staining. We found that there was a significant increase in the infarct volume of *Prdx1*$^{-/-}$ mice (Fig. 3A). Moreover, neurological deficit scores and motor tests revealed that stroke outcomes in *Prdx1*$^{-/-}$ mice were significantly exacerbated compared to those seen in *Prdx1*$^{+/+}$ mice (Fig. 3B). In contrast, baseline performance measured by rota-rod pretest did not differ between non-stroke *Prdx1*$^{-/-}$ mice and non-stroke *Prdx1*$^{+/+}$ mice (Supplementary Table 2). Nissl staining, Evans blue and Microfil staining in the homeostatic brain showed no difference in brain cell morphology and blood vessel leakage in artery function (Supplementary Fig. S3). Also, blood flow velocity and cerebral carotid artery (CCA) diameter were not different between *Prdx1*$^{+/+}$ and *Prdx1*$^{-/-}$ mice before the tMCAO surgery (Supplementary Table 3), suggesting that Prdx1 depletion has no effect on the pre-stroke phenotype. At 72 h post-stroke onset, the survival rate significantly decreased in the *Prdx1*$^{-/-}$ mice, indicating that *Prdx1* conferred protection against stroke I/R damage and is essential for cell survival in the brain (Fig. 3C). In contrast to *Prdx1*$^{-/-}$ mice, *Prdx2*$^{-/-}$ mice did not show an increase in infarct size after stroke (Supplementary Fig. S4A), supporting the previous reports that differences are seen in the pathological properties of the six subtypes of PRDX (Prdx1-6) [28,29,54].

TUNEL assays and crystal violet staining performed with *Prdx1*$^{+/+}$ and *Prdx1*$^{-/-}$ mouse brain slices confirmed that more cell death occurred in *Prdx1*$^{-/-}$ mice (Fig. 3D and E). To investigate the different responses of microglia in *Prdx1*$^{+/+}$ and *Prdx1*$^{-/-}$ mouse brain slices, we performed FACS analysis for the microglial marker, CD45^{+}, and CD11b^{+}. We found that the number of microglia was reduced in the IL hemisphere of *Prdx1*$^{-/-}$ mice compared to that of *Prdx1*$^{+/+}$ mice (Fig. 3F). FACS results with Annexin V-APC, and PI staining in microglia showed increased microglial cell death in the *Prdx1*$^{-/-}$ ipsilateral hemisphere compared to *Prdx1*$^{+/+}$ microglia (Fig. 3G). In support of these results, immunohistochemical analysis showed that cerebral ischemic stroke led to a significant increase of c-Caspase 3-positive cell number in the IL hemisphere of *Prdx1*$^{-/-}$ mice *in vivo* (Fig. 3H). We also substantiated these findings using *in vitro* oxygen-glucose deprivation/reoxygenation (OGD/R), in which BV-2 cells were subjected to hypoxia for 5 h under an acidotic condition in a hypoxia chamber and then reperfused for 24 h in a reperfusion system to mimic ischemic stroke brain damage. BV-2 cell viability was decreased at si-Prdx1 treated group compared to control siRNA group (Supplementary Figs. S4B and C). Crystal violet staining for BV-2 cell viability showed that OGD/R significantly decreased the population of crystal violet-positive cells (Supplementary Fig. S4D). siRNA-mediated knockdown of *Prdx1* further reduced the crystal violet-positive cells in this system, while adenovirus-induced overexpression of *Prdx1* recovered the crystal violet-positive cells to a level comparable to that seen in a control siRNA group (Supplementary Fig. S4D). Although there are limitations to mimic *in vivo* experiments, these results partially support that Prdx1 in microglia is required for controlling oxidative stress. Ferrostatin-1 (Fer-1), which is an inhibitor of ferroptosis, had no effect on *Prdx1*-associated cell death, suggesting that *Prdx1*-dependent protection does not involve the suppression of ferroptosis (Supplementary Fig. S4C).

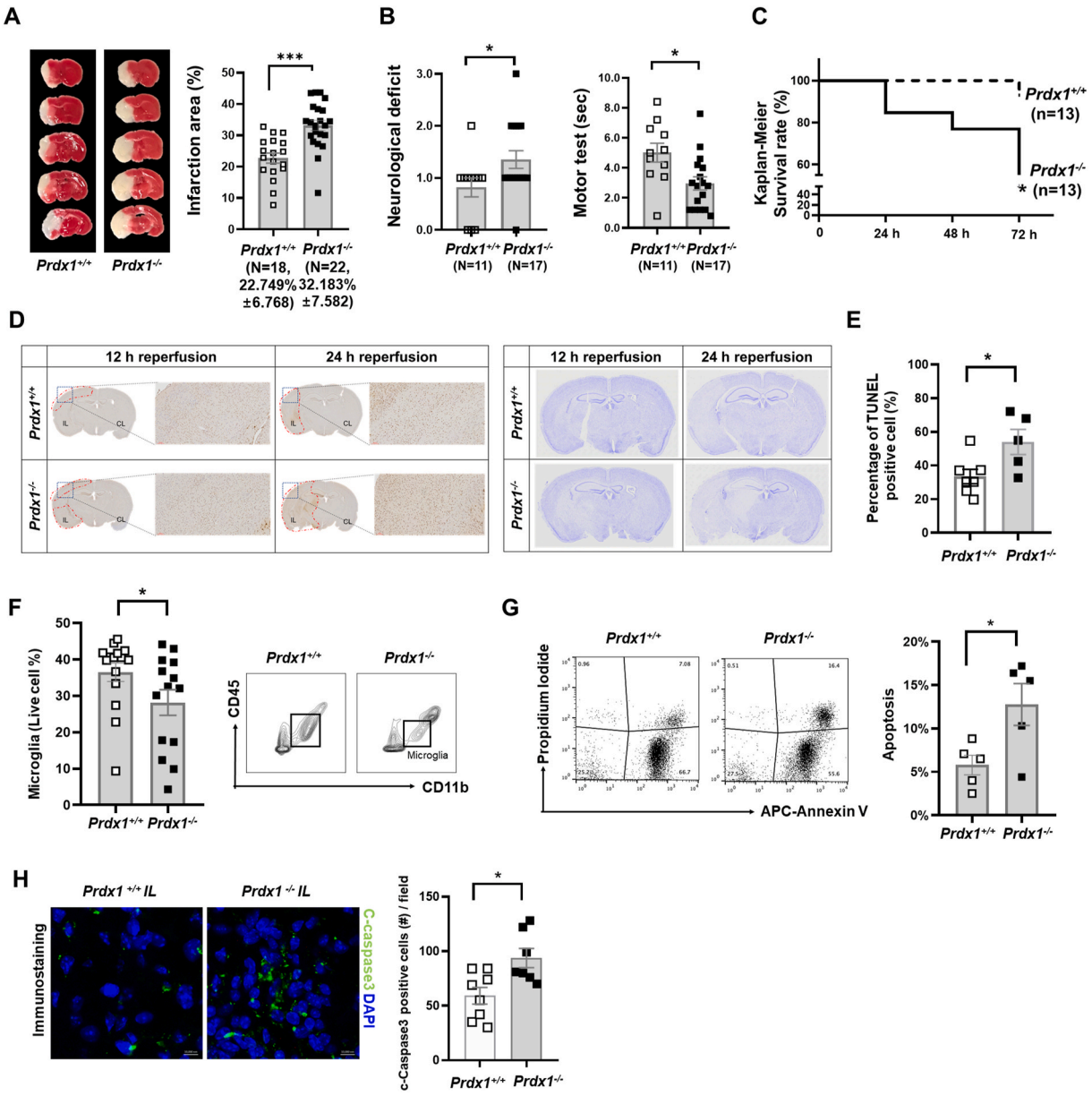

Fig. 3. Peroxiredoxin1 (Prdx1) deficiency exacerbates brain damage after stroke onset. (A) Representative images of TTC stained brain slices of *Prdx1*+/+ (n = 18) and *Prdx1*−/− (n = 22) mice. Bar graph showed quantification of infarct volume. **(B)** Neurologic scores (see Methods) for *Prdx1*+/+ (n = 11) and *Prdx1*−/− (n = 17) mice (left panel). Motor test scores (sec) for *Prdx1*+/+ (n = 11) and *Prdx1*−/− (n = 17) mice. **(C)** Kaplan-Meier Survival rates (Gehan-Breslow-Wilcoxon test) of *Prdx1*+/+ (n = 13) and *Prdx1*−/− (n = 13) mice at 24 h, 48 h, and 72 h after reperfusion. **(D)** TUNEL assay (left panel) and crystal violet staining (right panel) of ischemic brain at 12 h and 24 h after ischemic stroke (*Prdx1*+/+: n = 7, *Prdx1*−/−: n = 5). **(E)** Bar graphs displaying the percentage of TUNEL-positive cells in *Prdx1*+/+ and *Prdx1*−/− mouse brains. **(F)** FACS analysis showing the proportion of microglia in the whole live cells of IL hemispheres of *Prdx1*+/+ (n = 13) and *Prdx1*−/− (n = 14) mice. **(G)** FACS analysis showing Annexin V/PI staining in *Prdx1*+/+ (n = 5) and *Prdx1*−/− (n = 5) ipsilateral microglia population. The bar graph showing the ration of apoptosis among in *Prdx1*+/+ and *Prdx1*−/− microglia. **(H)** Representative immunofluorescence images (X400) of c-caspase3 staining in the infarction regions of *Prdx1*+/+ and *Prdx1*−/− mice. (A), (B), (E), (F), (G) and (H) mice were used at 24 h after ischemia. Data were presented mean SEM analyzed by unpaired two-tailed Student t-test $*P<0.05$, $**P<0.01$, $***P<0.001$. *(For interpretation of the references to colour in this figure legend, the reader is referred to the Web version of this article.)*

3.4. SAM are activated to protect against I/R injury via Prdx1-dependent pathways

The enrichment of antioxidant genes in SAM suggested that SAM activation upon stroke may be linked to *Prdx1*-dependent pathways. To address this hypothesis, we performed scRNA-seq with IL hemispheres of *Prdx1*$^{-/-}$ mice and integrated the obtained data with the previous data set (Fig. 2) to analyze SAM activation. Since we analyzed more cells (n = 39,956), the unbiased UMAP plot allowed us to distinguish cell populations with higher resolution and provided detailed information about cell-to-cell heterogeneity (Fig. 4A). Similar to the previous results (Fig. 2), we observed that microglial cell death and infiltrated immune cells were significantly increased in the IL hemisphere of *Prdx1*$^{-/-}$ mice (Fig. 4B). To examine SAM activation in the absence of *Prdx1*, we again performed the subclustering analysis with a merged microglial data set (Fig. 4C). Three different subclusters were found to be differently regulated under Prdx1 depletion; of them, cluster 3 was annotated as corresponding to SAM based on the gene expression patterns. The numbers of microglia in clusters 1 and 2 showed little change, whereas cluster 3 (SAM) comprised significantly fewer microglia in *Prdx1*$^{-/-}$ IL

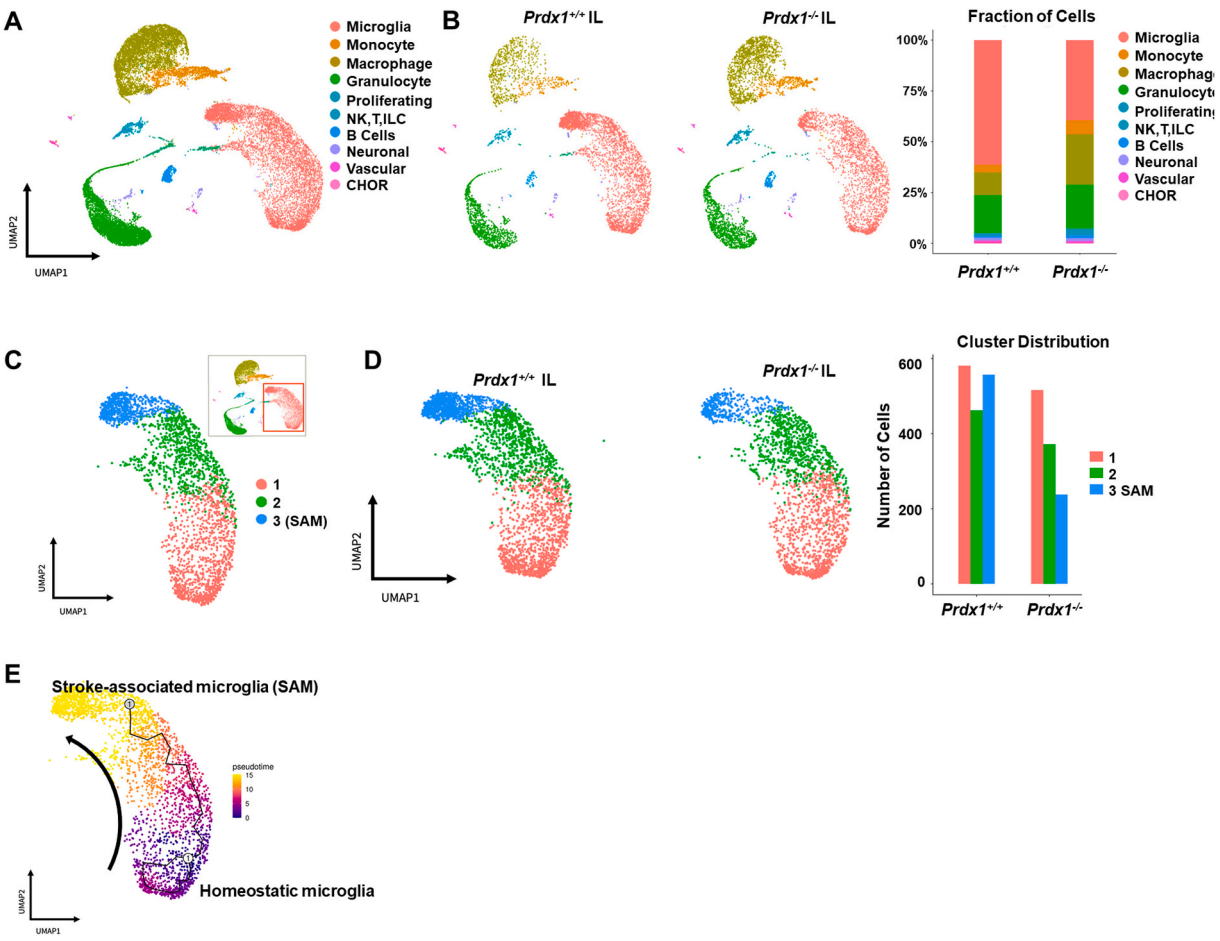

Fig. 4. Prdx1 is essential for SAM activation after stroke damage. (A) UMAP plots showing clusters and annotations of cells identified in *Prdx1*+/+ and *Prdx1*−/− IL hemispheres after tMCAO. (39,956 cells) **(B)** UMAP plots showing immune cells clusters in *Prdx1*+/+ (*WT* IL) or *Prdx1*−/− (*KO* IL) IL hemispheres at 24 h after tMCAO (left panel). Bar plot showing the relative distribution of each cluster identified in the *Prdx1*+/+ (*WT*) and *Prdx1*−/− IL (*KO*) hemispheres at 24 h after tMCAO (right panel). **(C)** Subclustering analysis of the microglia identified in (A). **(D)** UMAP plots of microglial subclusters in the *Prdx1*+/+ (*WT* IL) and *Prdx1*−/− IL (*KO* IL) hemispheres (left panel). Stacked bar graph showing the number of microglia counted from the *Prdx1*+/+ (*WT*) and *Prdx1*−/− IL (*KO*) hemispheres at 24 h after tMCAO (left panel). **(E)** Projection of microglia on a pseudo-time graph plot displaying the transition from homeostatic microglia (clusters 1 and 2, blue) to SAM (cluster 3, yellow). (For interpretation of the references to colour in this figure legend, the reader is referred to the Web version of this article.)

compared to *Prdx1*$^{+/+}$ IL (Fig. 4D). Our pseudo-time analysis revealed a trajectory from cluster 1 to SAM (Fig. 4E) that was similar to the one described above and shown in Fig. 2D. These results suggest that SAM activation is dependent on Prdx1 and the specific reduction of SAM is associated with ischemic brain injury and microglial cell death in the IL hemisphere of *Prdx1*$^{-/-}$ mice.

Next, we investigated the antioxidant properties of the newly defined SAM cluster (cluster 3) derived from the integrated data set. In support of the phenotype observed *in vivo*, these SAM showed highly elevated expression levels of antioxidant genes, including *Prdx1, Txn1, Srxn1,* and *Mt1/2*, compared to the levels seen in homeostatic microglia (Fig. 5A). Scatterplots of the normalized gene expression in SAM (cluster 3) against those of homeostatic microglia (cluster 1 and 2) showed that there was some differential gene expression in SAM (Fig. 5B and Supplementary Table 1). GO analysis revealed that antioxidant systems, extracellular matrix binding, and cytokine activity were activated in SAM (Fig. 5C). We corroborated this understanding of SAM signaling using a ranked metric pathway list (Fig. 5D) and found that the SAM-enriched genes converged as molecular pathways associated with oxidoreductase activity (Fig. 5E). To further assess the defective anti-oxidative properties of *Prdx1*-deficient microglia, we measured ROS stress response molecules in the damaged microglia, because high ROS is widely regarded as being involved in the initiation of ischemic damage. FACS analysis using two different fluorescent probes, C11-BODIPY (Fig. 5F) and H_2DCFDA (Fig. 5G), demonstrated that ischemic I/R damage increased ROS generation in IL microglia compared to CL microglia and that *Prdx1*-deficient microglia exhibited further enhancement of ROS accumulation under ischemic I/R damage. Comparative analysis with DAM verified that SAM shared markers that are either down-regulated or up-regulated in DAM, indicating that SAM represent a microglial population different from homeostatic microglia of clusters 1 and 2 in the IL hemisphere microglia population (Fig. 5H). Together, our findings indicated that SAM are activated by *Prdx1*-dependent pathways and that loss of *Prdx1* specifically decreases the number of SAM, but not homeostatic microglia, contributing to overall increased microglial cell death and exacerbation of ischemic injury. SAM share similar markers with DAM but differ from DAM in exhibiting enriched antioxidant properties, implying that SAM are specialized microglia in ischemic stroke.

3.5. *Infiltrated immune cells minimally affect ischemic brain injury in the acute phase*

Immune cell infiltration after an ischemic injury has long been considered to increase tissue damage, such as through the production of proinflammatory cytokines [55]. Cerebral ischemia triggers an inflammatory response that is controlled by the activation of resident microglia and the infiltration of peripheral myeloid and lymphoid cells into the IL

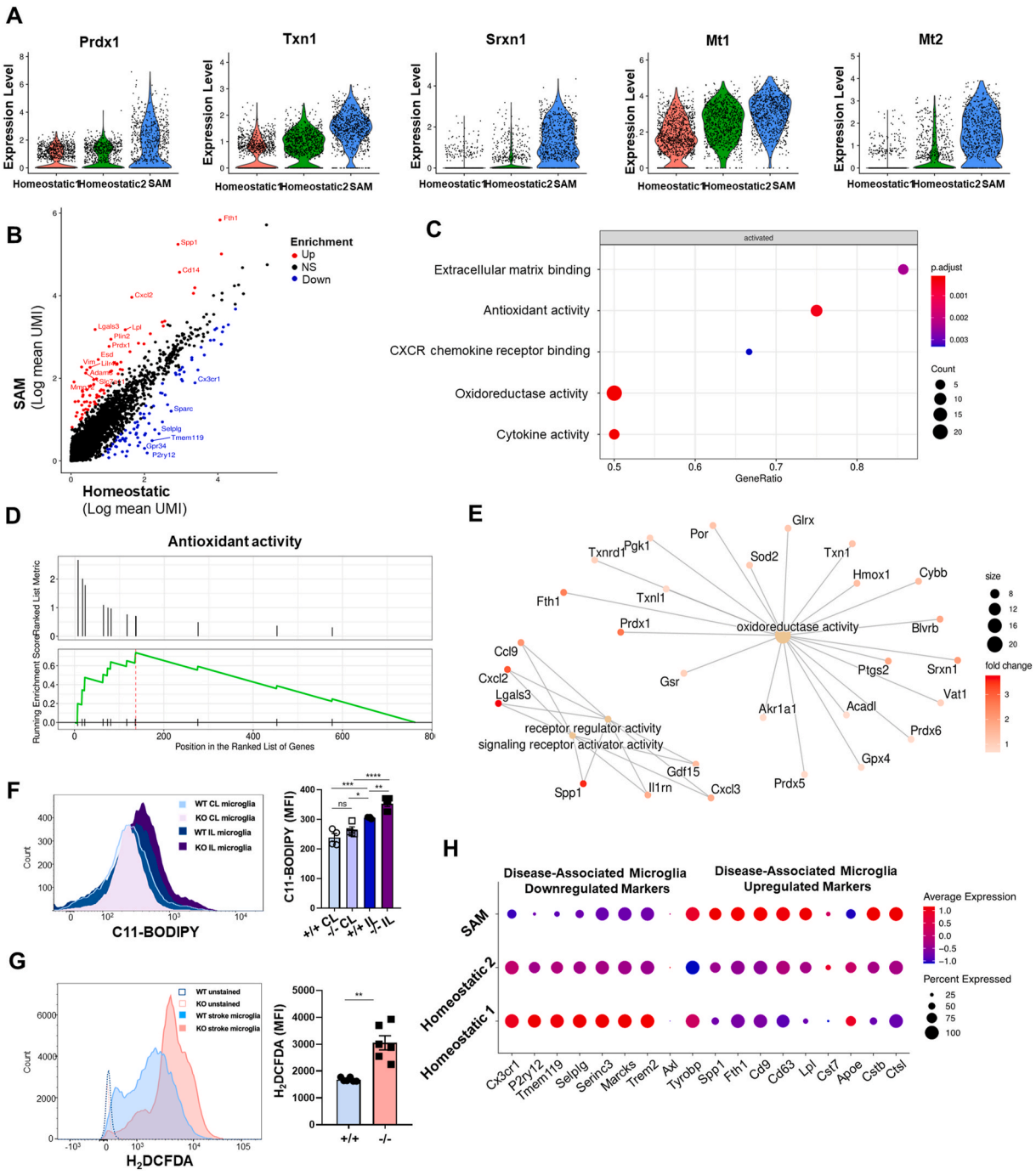

Fig. 5. SAM exhibit enhanced antioxidative activity along with several DAM markers. (A) Violin plots showing gene expression levels of the indicated genes in homeostatic clusters 1 and 2 and SAM. **(B)** Scatterplot showing scRNA-seq analysis of differentially expressed genes. Red and blue dots indicate genes that were significantly increased and decreased in SAM, respectively (log2FC>±1.5). **(C)** Dot plots indicating activated pathways of SAM in the IL hemisphere. **(D)** GSEA pathway analysis of differentially expressed genes in SAM. **(E)** KEGG pathway analysis showing enriched pathways in SAM. **(F, G)** FACS analysis showing BODIPY 581/591 MFI (Mean Fluorescence Intensity) of *Prdx1*+/+ IL and *Prdx1*−/− IL microglia **(F)** and H2DCFDA of *Prdx1*+/+ IL and *Prdx1*−/− IL microglia staining **(G)** after 24 h in stroke microglia. Data are presented as mean ± SEM and were analyzed by the 2-way ANOVA test and unpaired two-tailed Student's t-test, $*P<0.05$, $**P<0.01$, $***P<0.001$. **(H)** Expression of DAM marker genes in SAM and homeostatic microglia obtained from the *Prdx1*+/+ and *Prdx1*−/− IL hemispheres at 24 h after tMCAO. Red or blue lines respectively indicate up-regulated or down-regulated marker genes of DAM. Increased or decreased gene expression in SAM versus homeostatic microglia is indicated by red or blue dots, respectively. . (For interpretation of the references to colour in this figure legend, the reader is referred to the Web version of this article.)

hemisphere [56]. Our scRNA-seq results revealed decreased microglia and increased infiltration of immune cells, especially that of macrophages and granulocytes in the *Prdx1*$^{-/-}$ mouse IL hemisphere compared with the *Prdx1*$^{+/+}$ mouse IL hemisphere after tMCAO surgery (Fig. 1E–G and Fig. 4). FACS analysis with known markers (Supplementary Fig. S1C) confirmed that there were more infiltrated macrophages in the *Prdx1*$^{-/-}$ mouse IL hemisphere compared to the *Prdx1*$^{+/+}$ mouse IL hemisphere at 24 h after infarction (Fig. 6A). Ischemic I/R damage increased the serum levels of Il-1β, Ccl2, and Il-6, and these cytokines were further increased in the *Prdx1*$^{-/-}$ mice

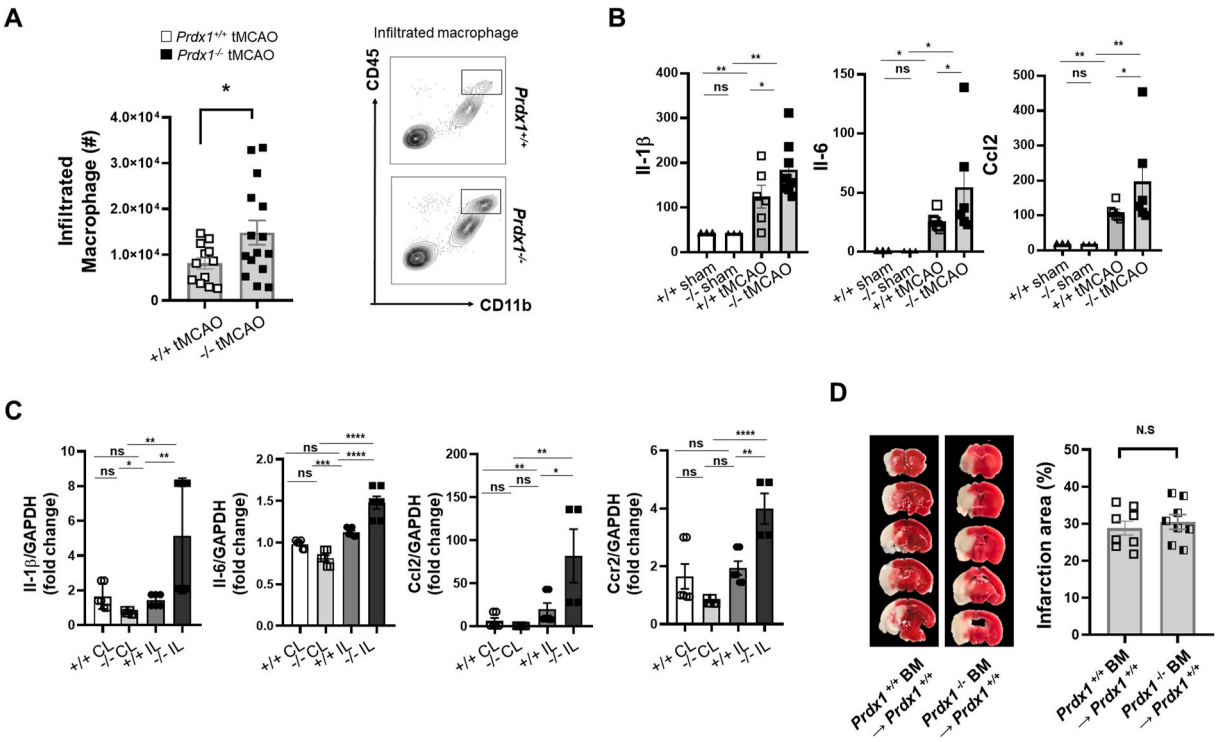

Fig. 6. Prdx1 expression of resident microglia is required for protecting the brain against acute stroke damage. (A) FACS analysis of CD45hi, CD11b + infiltrated macrophages in the *Prdx1*+/+ (n = 12) and *Prdx1*−/− (n = 15) IL hemispheres. **(B)** ELISA (n > 5 per group) and **(C)** real-time PCR (n = 3 per group) analyses of inflammatory cytokines and chemokines, including Il-1, Il6, Ccl2, and Ccr2. Data were presented mean SEM and analyzed by 2-way ANOVA test. **(D)** Representative images of TTC stained brain slices from bone marrow transplantation (BMT) mice. BM from *Prdx1*+/+ (n = 8) and *Prdx1*−/− (n = 8) mice were transplanted into *WT* recipients. Bar graph showed quantification of infarct area for BM from *Prdx1*+/+ and *Prdx1*−/−. All of mice were used at 24 h after tMCAO. Data were presented mean SEM and analyzed by unpaired two-tailed Student t-test, $*P<0.05$, $**P<0.01$, $***P<0.001$.

subjected to stroke (Fig. 6B). Consistently, the gene expression levels of *Il-1β, Ccl2, Il-6*, and *Ccr2* were significantly increased in the IL hemisphere of *Prdx1*$^{-/-}$ mice, suggesting that the infiltrated immune cells play a pro-inflammatory role under ischemic injury (Fig. 6C). To further investigate the effect of infiltrated pro-inflammatory immune cells on brain injury, we performed bone marrow transplantation to separate the effect of Prdx1 expression by resident microglia from that of infiltrated immune cells. Unexpectedly, *Prdx1*$^{+/+}$ mice transplanted with bone marrow (BM) from *Prdx1*$^{-/-}$ mice did not exhibit any significant increase in the infarct volume compared to *Prdx1*$^{+/+}$ BM-transplanted recipients (Fig. 6D). However, bioinformatic analysis of the DEG of macrophages, monocytes, and granulocytes showed that ischemic injury in *Prdx1*$^{-/-}$ mice caused up-regulation of antioxidant, peroxidase, cytokine, and immune activities (Supplementary Figs. S5A and B). These data suggest that the exacerbation of brain damage in *Prdx1*$^{-/-}$ mice minimally involved by infiltrated immune cells despite our observation of increased inflammatory responses, at least at 24 h after tMCAO. Within this time window, *Prdx1*-dependent stroke damage is mainly mediated by microglial responses. Infiltrated immune cells are expected to play roles in the late phase, as previously reported [49,57]. However, since most of the *Prdx1*$^{-/-}$ mice died within 3 days after tMCAO surgery (Fig. 3C), the effect of peripheral immune cells in *Prdx1*$^{-/-}$ mice remains unclear in our experimental setting.

3.6. Antioxidant SAM are Spp1/Fth1-positive protective microglia

To examine additional potential features of SAM beyond their antioxidant functions, we further analyzed the single-cell data for other specialized function-related markers over-represented in SAM. Comparison of the homeostatic clusters with that representing SAM revealed that the expression of *Spp1*, which encodes osteopontin (OPN), was significantly increased in SAM (Fig. 7A). OPN has pleiotropic immunomodulatory functions, and its neuroprotective and reparative capacity has been implicated in ischemic stroke [58,59]. FACS analysis (Fig. 7B) and immunostaining (Fig. 7C) showed that SAM express OPN in IL hemisphere and Spp1 positive microglia were further decreased in *Prdx1*$^{-/-}$ mice. Immunoblot analysis showed that the expression of Spp1 was decreased in microglia from the *Prdx1*$^{-/-}$ IL hemisphere compared to *Prdx1*$^{+/+}$ IL microglia (Fig. 7G), suggesting that *Spp1* in microglia is regulated by *Prdx1*-dependent antioxidant pathways.

The high-level expression of the *Spp1* gene in SAM and the decreased expression level observed in *Prdx1*$^{-/-}$ microglia suggest that SAM are important cellular sources of OPN. Secreted OPN has been shown to interact with integrin receptors and *Cd63* on microglia to intensify the reparative capacity [60,61]. In support of this, we found that SAM expressed high levels of *Itga5* and *Cd63* with no change in *Itgb1* (Fig. 7D), suggesting that intrinsic and extrinsic actions of OPN may play protective roles in acute ischemic brain injury. Our IHC data confirmed that SAM express Cd63 after stroke damage (Fig. 7E).

Fth1 (Ferritin1) was another marker found to be specifically upregulated in SAM relative to the other tested cell populations. The scRNA-seq data showed that SAM expresses increased levels of *Fth1* and *Ftl1*, which activates *Fth1* to form functional ferritin (Fig. 7F). Immunoblot analysis showed that the expression of Fth1 was decreased in microglia from the *Prdx1*$^{-/-}$ IL hemisphere (Fig. 7G). Interestingly, co-expression analysis revealed that *Fth1* expression was highly correlated with that of *Cd63* (Fig. 7H), indicating that *Fth1* and *Cd63*, as well as *Prdx1*-dependent pathways, could be potential markers for distinguishing SAM from other homeostatic microglia or even DAM. FACS histogram showed that both Cd63 and Fth1 expression were increased after stroke damage and Prdx1 depletion decreased the MFI value of the SAM markers in ipsilateral microglia population (Fig. 7I). Prdx1-dependent Fth1/Cd63 double-positive SAM were verified with FACS analysis (Fig. 7J) and immunohistochemistry (Fig. 7K). Importantly, triple-immunostaining

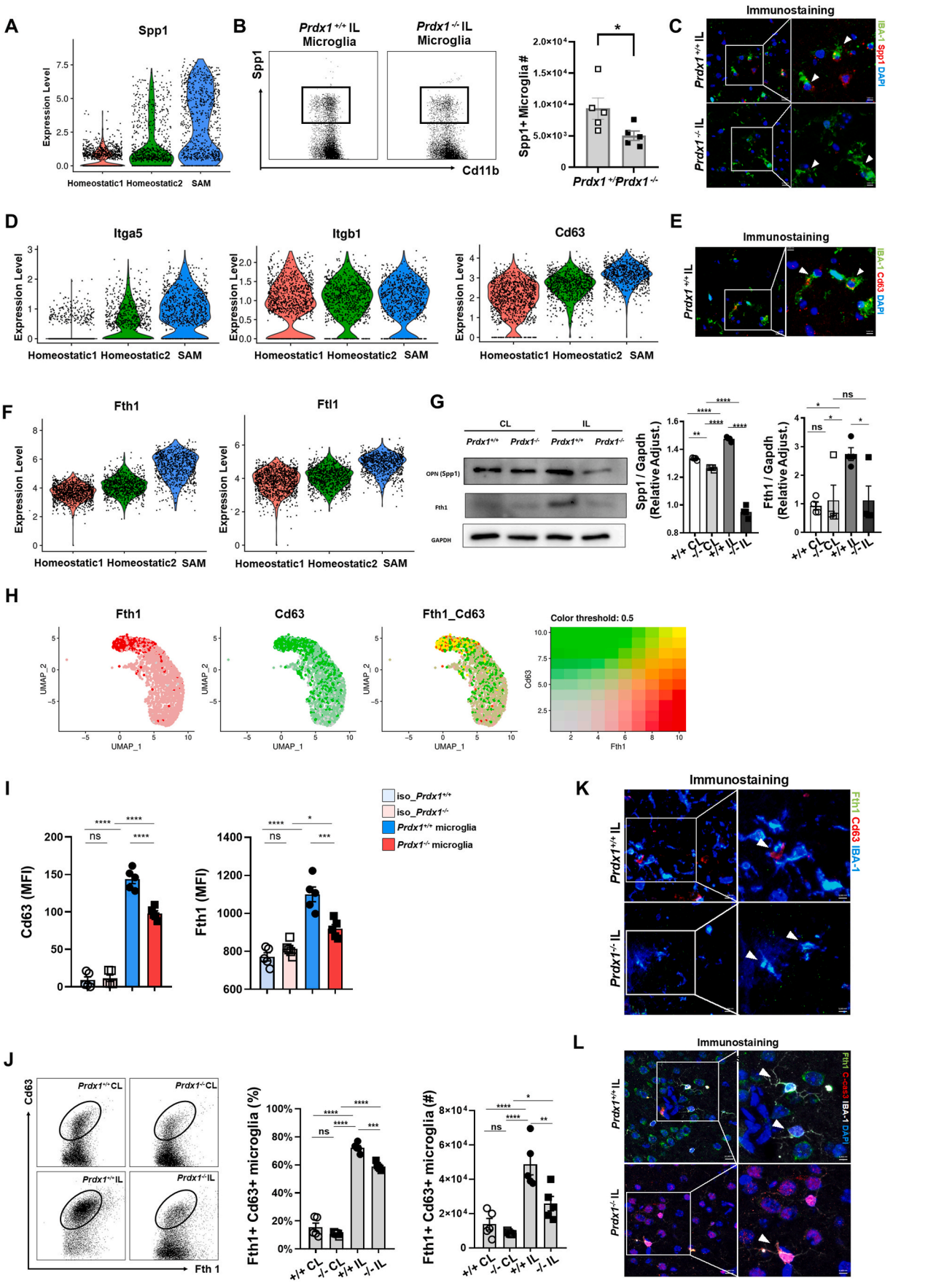

(caption on next page)

Fig. 7. SAM are potential protective microglia associated with ischemic stroke. (A) Violin plots showing the expression of *Spp1* in homeostatic clusters 1 and 2 and SAM. **(B)** FACS analysis of Spp1 positive microglia population in the IL hemisphere of *Prdx1*+/+ (n = 5) and *Prdx1*−/− (n = 5) mice after tMCAO. **(C)** Representative IHC images for Spp1 positive SAM population in the ipsilateral hemisphere of *Prdx1*+/+ and *Prdx1*−/− mice. **(D,F)** Violin plots showing gene expression levels of the indicated genes in homeostatic clusters 1 and 2 and SAM. **(E)** Representative IHC images for Cd63 positive SAM population in the ipsilateral hemisphere of *Prdx1*+/+ mice. **(G)** Immunoblot analysis of Spp1 and Fth1 in CL and IL hemispheres of *Prdx1*+/+ and *Prdx1*−/− mice at 24 h after tMCAO (n = 4). Bar graph showing quantification of blotting images. **(H)** UMAP plots showing co-expression of *Fth1* (red) and *Cd63* (green). **(I)** FACS analysis showing Cd63 and Fth1 expression of *Prdx1*+/+ IL microglia and *Prdx1*−/− IL microglia the indicated conditions. Data are presented as Mean Fluorescence Intensity (MFI). **(J)** FACS analysis of Fth1, Cd63 double positive SAM population proportion and numbers in the IL hemisphere of *Prdx1*+/+ (n = 5) and *Prdx1*−/− (n = 5) mice. **(K)** Representative IHC images for Cd63, Fth1 double positive SAM population in the IL hemisphere of *Prdx1*+/+ and *Prdx1*−/− mice. **(L)** Representative IHC images for Fth1 and c-Caspase3 in infarct regions of *Prdx1*+/+ and *Prdx1*−/− microglia (IBA-1). All of mice were used at 24 h after tMCAO. Data were presented mean SEM and analyzed by 2-way ANOVA test or the unpaired two-tailed Student's t-test, $*P<0.05$, $**P<0.01$, $***P<0.001$. *(For interpretation of the references to colour in this figure legend, the reader is referred to the Web version of this article.)*

with SAM marker Fth1, microglia marker IBA-1, and apoptosis marker cleavage-Caspase3 revealed that Fth1 expression was increased in microglia of the damaged IL hemisphere of *Prdx1*$^{+/+}$ mice, whereas Prdx1 depletion decreased Fth1 expression and increased cleavage-Caspase3 expression (Fig. 7L). Overall, our results suggest that SAM activation is initiated by antioxidant Prdx1 pathways and is coupled to genes that are protective against ischemic brain injury, such as *Spp1* and *Fth1*. SAM are associated with the limitation of ischemic damage and thus have important implications for treating acute stroke.

4. Discussion

Here, we comprehensively identified the transcriptome of microglia as they progressed from homeostatic clusters to a unique type of microglia that have *Prdx1*-dependent antioxidant actions in acute I/R injury. We identified a population of microglia that showed a stroke-specific phenotype, and termed them SAM. Our further experiments revealed that *Prdx1*-dependent antioxidant pathways are required for both activating SAM and restricting oxidative stress in early-stage stoke, and that SAM are essential components of the immune responses that protect the brain against acute I/R brain injury. We suggest that SAM represent a specialized and unique type of microglia that resemble DAM and act to limit oxidative stress and cell death under acute ischemia.

The CNS and the immune system are tightly interconnected through complex communication networks. Microglia are resident CNS immune cells that function as active sensors in a healthy brain and as versatile effectors under pathological conditions [62]. In contrast, macrophages surround the blood vessels and line the leptomeninges and the choroid plexus; along with dendritic cells and lymphocytes, they contribute to immunosurveillance [5,63]. The immune system closely monitors brain function and responds when brain homeostasis is lost due to injury or disease. While seminal studies have increased our understanding of ischemic brain damage, the ischemic hemisphere-specific roles of microglia and immune cells remain elusive. Cerebral ischemia is known to induce ROS-mediated damage, including marked changes in the phenotypes of various endogenous CNS cell types [12,13]. Understanding how microglia become dysregulated and respond to the oxidative stress caused by ROS production is crucial to understanding inflammatory-associated neurodegeneration [6,64]. However, heterogeneous microglia capable of protecting against stroke damage have not previously been investigated on a single-cell level. Moreover, little was known about gene-specific regulation of microglia subclusters during stroke infarction. Our scRNA-seq analysis in tMCAO model mice revealed that single-cell analysis of stroke brain cells can be a highly effective method for isolating all types of immune cell populations from stroke brains.

Importantly, we identified novel clusters of microglia that we called SAM and showed that they are expanded in acute I/R stroke compared to the populations of homeostatic microglia. In the IL hemisphere, the total cell number of microglia was greatly decreased by acute I/R injury, but the number of SAM was rather increased at 24 h after surgery. These results suggest that a switching of major microglial populations was intrinsically induced as a means to respond to oxidative stress and ROS damage. SAM expressed high levels of antioxidant molecules, including *Prdx1, Txn1, Srxn1*, and *Mt1/2*. In addition to high-level activation of antioxidant pathways, SAM showed a gene expression pattern similar to that previously reported for the protective DAM activated in AD and ALS. DAM are phagocytic cells that are conserved in neurodegenerative diseases and activated sequentially by *Trem2*-independent and -dependent pathways [18]. SAM have a low *Trem2* level, but otherwise their gene expression pattern is relatively similar to that of DAM; thus, SAM appear to resemble *Trem2*-independent stage 1 DAM. Collectively, these findings imply that microglia are reprogrammed to be disease-specific under various pathological conditions, and that SAM are generated as a response to prepare for stroke ischemia. In this study, we identified representative markers of SAM. Currently, however, canonical marker-based cell isolation is technically challenging for microglial populations. Both DAM and SAM show down-regulation of microglial markers, such as *Cx3cr1, Trem2*, and *Tmem119*, and it is quite difficult to isolate microglia or SAM with low expression of classical microglia markers. In addition, some genes we found to be characteristic of SAM are not suitable for sorting. Therefore, new methods are needed to isolate those unusual cells to enable more detailed studies on the mechanisms of SAM.

Brain cells are susceptible to oxygen deficiency, which increases ROS levels and subsequent oxidative stress, brain cell damage, and blood-brain barrier dysfunction [6,65]. In this study, we demonstrated that the presence of the typical antioxidant gene, *Prdx1*, protects against acute I/R injury and is required for SAM activation and the consequent reduction of microglial cell death and inflammatory responses. However, *Prdx1* is expressed in many cell types throughout the brain [28], and our experimental model using conventional *Prdx1*$^{-/-}$ mice is limited in elucidating the role of microglia-specific *Prdx1*. Indeed, it is not clear whether the observed results are primary effects from microglia *Prdx1* or secondary effects from other CNS or peripheral cells. But *Prdx1* deficiency specifically diminished the SAM population that would normally expand under I/R injury and increased microglial cell death along with decreased SAM markers predicted by scRNA-seq. The result of bone marrow transplantation separated the effect of Prdx1 by resident microglia from that of infiltrated immune cells although we have not entirely ruled out a mixed effect from microglia and non-microglia brain cells. In addition, *in vitro* data on BV-2 cell line after OGD partially support the role of Prdx1 in microglia. Taken together, these results suggest that Prdx1 is required for SAM activation with strong antioxidant function and is essential for proper responses to environmental sues such as stroke.

We found that *Prdx1*$^{-/-}$ mice were more severely injured by acute I/R injury, as confirmed by TTC staining, neurological deficit scores, motor tests, and the survival rate, indicating that *Prdx1* has a protective function. Other studies have yielded contradictory results regarding the impact of *Prdx1* on stroke damage [35,36]. This is mainly because Prdx1 can decrease oxidative stress through its intracellular antioxidant function, but it can also increase the inflammatory response by acting as a DAMP that can be expelled from the cell and recognized through TLR. For example, Shichita et al. [29]. showed that the extracellular release of Prdx family proteins from necrotic brain cells induced expression of

inflammatory cytokines, promoting neural cell death. However, the same authors observed and discussed the exacerbation of ischemic damage in *Prdx1*$^{-/-}$ mice, although no data was presented in this paper. This strongly indicates that the intracellular role of Prdx1 should be distinguished from its extracellular role, and provides additional evidence that loss of *Prdx1* exacerbates acute I/R injury. The specific decrease of SAM in *Prdx1*$^{-/-}$ mice observed herein suggests that SAM are activated by intracellular Prdx1 to regulate ROS stress at the damaged brain.

The findings that stroke-protective genes, such as *Spp1, Itga5, Cd63*, and *Ftn1*, showed *Prdx1*-dependent expression in SAM may give us a clue about the physiological functions of SAM as brain-protective cells, beyond their ROS-scavenging functions. We also demonstrated that SAM express Spp1, Cd63, Fth1 proteins and Prdx1 depletion reduced the SAM marker with increased apoptosis. A recent study showed that OPN secreted from regulatory T cells in the late phase of stroke stimulated microglia, promoting oligodendrogenesis and recovery processes [58]. Injury-responsive microglia were shown to increase transcription of *Spp1* in demyelinated lesions, and incubation of cortical neuron cultures with OPN reportedly prevented oxygen and glucose deprivation from triggering cell death [66,67]. Although the molecular mechanisms underlying stroke damage are not well understood [68,69], ferritin is known to play a role in storing iron in a soluble and nontoxic state, and ferritin deficiency has been associated with several neurodegenerative diseases [70]. It has been shown that DAM, which shared many gene expression with SAM, has a protective role in neurological disease, providing hints about the 'potential protective role of SAM'. Therefore, *Prdx1*-dependent SAM may also contribute to sustaining the reparative capacity and interacting with infiltrated immune cells. Neuroprotection by *Prdx1*-dependent SAM may involve the antioxidant function in the context of tissue remodeling, inflammatory responses, anti-apoptotic actions, and other mechanisms, such as the proliferation of nerve cells.

In summary, we herein show that *Prdx1* protects against microglial cell death under ischemia and modulates the immune response by generating a new cluster of microglia, SAM, in the IL hemisphere. We suggest that *Prdx1* affects the cell death mechanisms of brain-resident cells and could be an essential target protein for reducing ischemic stroke damage. *Prdx1*-dependent SAM may be a potential biomarker and therapeutic target for protecting microglial function and treating brain I/R injury. Although this new cluster will require further study, our findings provide a new perspective: that Prdx1-mediated microglial heterogeneity is important in ischemic stroke.

Author contributions

S.K., W.L, S.H.P, and G.T.O proposed the concept, contributed to the study design, and wrote the manuscript with help from the other authors. All authors actively discussed and reviewed the manuscript.

Declaration of competing interest

We declare that there are no conflicts in interest.

Acknowledgements

This work was supported by National Research Foundation of Korea (NRF) grants funded by the Korean government (MSIP; No. 2020RIA3B2079811, No. 2021M3E5E7023628, No. 2020R1A2C1006101, and No. 2018R1A5A1024340).

Appendix A. Supplementary data

Supplementary data to this article can be found online at https://doi.org/10.1016/j.redox.2022.102347.

References

[1] B.C.V. Campbell, et al., Ischaemic stroke, Nat. Rev. Dis. Prim. 5 (1) (2019) 70.
[2] C.L. Allen, U. Bayraktutan, Oxidative stress and its role in the pathogenesis of ischaemic stroke, Int. J. Stroke 4 (6) (2009) 461–470.
[3] A.I. Rojo, et al., Redox control of microglial function: molecular mechanisms and functional significance, Antioxidants Redox Signal. 21 (12) (2014) 1766–1801.
[4] H. Mathys, et al., Single-cell transcriptomic analysis of Alzheimer's disease, Nature 570 (7761) (2019) 332–337.
[5] M.J.C. Jordao, et al., Single-cell profiling identifies myeloid cell subsets with distinct fates during neuroinflammation, Science 363 (6425) (2019).
[6] A.S. Mendiola, et al., Transcriptional profiling and therapeutic targeting of oxidative stress in neuroinflammation, Nat. Immunol. 21 (5) (2020) 513–524.
[7] H.J.R. Fernandes, et al., Single-cell transcriptomics of Parkinson's disease human in vitro models reveals dopamine neuron-specific stress responses, Cell Rep. 33 (2) (2020), 108263.
[8] V.H. Perry, J. Teeling, Microglia and macrophages of the central nervous system: the contribution of microglia priming and systemic inflammation to chronic neurodegeneration, Semin. Immunopathol. 35 (5) (2013) 601–612.
[9] T. Shichita, M. Ito, A. Yoshimura, Post-ischemic inflammation regulates neural damage and protection, Front. Cell. Neurosci. 8 (2014) 319.
[10] X. Hu, et al., Microglial and macrophage polarization-new prospects for brain repair, Nat. Rev. Neurol. 11 (1) (2015) 56–64.
[11] P. Androvic, et al., Decoding the transcriptional response to ischemic stroke in young and aged mouse brain, Cell Rep. 31 (11) (2020), 107777.
[12] K. Guo, et al., Single-cell RNA sequencing with combined use of bulk RNA sequencing to reveal cell heterogeneity and molecular changes at acute stage of ischemic stroke in mouse cortex penumbra area, Front. Cell Dev. Biol. 9 (2021), 624711.
[13] K. Zheng, et al., Single-cell RNA-seq reveals the transcriptional landscape in ischemic stroke, J. Cerebr. Blood Flow Metabol. (2021), 271678X211026770.
[14] M. Colonna, O. Butovsky, Microglia function in the central nervous system during health and neurodegeneration, Annu. Rev. Immunol. 35 (2017) 441–468.
[15] Q. Li, B.A. Barres, Microglia and macrophages in brain homeostasis and disease, Nat. Rev. Immunol. 18 (4) (2018) 225–242.
[16] H. Van Hove, et al., A single-cell atlas of mouse brain macrophages reveals unique transcriptional identities shaped by ontogeny and tissue environment, Nat. Neurosci. 22 (6) (2019) 1021–1035.
[17] T. Masuda, et al., Microglia heterogeneity in the single-cell era, Cell Rep. 30 (5) (2020) 1271–1281.
[18] H. Keren-Shaul, et al., A unique microglia type Associated with restricting development of Alzheimer's disease, Cell 169 (7) (2017) 1276–1290 e17.
[19] A. Deczkowska, et al., Disease-associated microglia: a universal immune sensor of neurodegeneration, Cell 173 (5) (2018) 1073–1081.
[20] J. Priller, M. Prinz, Targeting microglia in brain disorders, Science 365 (6448) (2019) 32–33.
[21] Z. Cao, et al., Unique subtype of microglia in degenerative thalamus after cortical stroke, Stroke 52 (2) (2021) 687–698.
[22] S.G. Rhee, et al., Intracellular messenger function of hydrogen peroxide and its regulation by peroxiredoxins, Curr. Opin. Cell Biol. 17 (2) (2005) 183–189.
[23] S.J. Jeong, et al., Deficiency of peroxiredoxin 2 exacerbates angiotensin II-induced abdominal aortic aneurysm, Exp. Mol. Med. 52 (9) (2020) 1587–1601.
[24] J.G. Park, et al., Peroxiredoxin 2 deficiency exacerbates atherosclerosis in apolipoprotein E-deficient mice, Circ. Res. 109 (7) (2011) 739–749.
[25] H.A. Woo, et al., Inactivation of peroxiredoxin I by phosphorylation allows localized H(2)O(2) accumulation for cell signaling, Cell 140 (4) (2010) 517–528.
[26] S.J. Jeong, et al., Prdx1 (peroxiredoxin 1) deficiency reduces cholesterol efflux via impaired macrophage lipophagic flux, Autophagy 14 (1) (2018) 120–133.
[27] S.J. Jeong, J.G. Park, G.T. Oh, Peroxiredoxins as potential targets for cardiovascular disease, Antioxidants 10 (8) (2021).
[28] M. Szeliga, Peroxiredoxins in neurodegenerative diseases, Antioxidants 9 (12) (2020).
[29] T. Shichita, et al., Peroxiredoxin family proteins are key initiators of post-ischemic inflammation in the brain, Nat. Med. 18 (6) (2012) 911–917.
[30] R.R. Tao, et al., Nitrosative stress induces peroxiredoxin 1 ubiquitination during ischemic insult via E6AP activation in endothelial cells both in vitro and in vivo, Antioxidants Redox Signal. 21 (1) (2014) 1–16.
[31] S. Richard, et al., Diagnostic performance of peroxiredoxin 1 to determine time-of-onset of acute cerebral infarction, Sci. Rep. 6 (2016) 38300.
[32] Y. Lu, et al., Peroxiredoxin 1/2 protects brain against H2O2-induced apoptosis after subarachnoid hemorrhage, Faseb. J. 33 (2) (2019) 3051–3062.
[33] G.Q. Yang, et al., Prdx1 reduces intracerebral hemorrhage-induced brain injury via targeting inflammation- and apoptosis-related mRNA stability, Front. Neurosci. 14 (2020) 181.
[34] C.H. Liu, et al., Peroxiredoxin 1 induces inflammatory cytokine response and predicts outcome of cardiogenic shock patients necessitating extracorporeal membrane oxygenation: an observational cohort study and translational approach, J. Transl. Med. 14 (1) (2016) 114.
[35] T. Shichita, et al., MAFB prevents excess inflammation after ischemic stroke by accelerating clearance of damage signals through MSR1, Nat. Med. 23 (6) (2017) 723–732.
[36] Q. Liu, Y. Zhang, PRDX1 enhances cerebral ischemia-reperfusion injury through activation of TLR4-regulated inflammation and apoptosis, Biochem. Biophys. Res. Commun. 519 (3) (2019) 453–461.

[37] Y.H. Han, et al., Peroxiredoxin I deficiency attenuates phagocytic capacity of macrophage in clearance of the red blood cells damaged by oxidative stress, BMB Rep 45 (10) (2012) 560–564.
[38] Y. Hao, et al., Integrated analysis of multimodal single-cell data, Cell 184 (13) (2021) 3573–3587 e29.
[39] C.S. McGinnis, L.M. Murrow, Z.J. Gartner, DoubletFinder: doublet detection in single-cell RNA sequencing data using artificial nearest neighbors, Cell. Syst. 8 (4) (2019) 329–337 e4.
[40] G. Yu, et al., clusterProfiler: an R package for comparing biological themes among gene clusters, OMICS 16 (5) (2012) 284–287.
[41] C. Trapnell, et al., The dynamics and regulators of cell fate decisions are revealed by pseudotemporal ordering of single cells, Nat. Biotechnol. 32 (4) (2014) 381–386.
[42] R.A. Swanson, et al., A semiautomated method for measuring brain infarct volume, J. Cerebr. Blood Flow Metabol. 10 (2) (1990) 290–293.
[43] Z. Huang, et al., Effects of cerebral ischemia in mice deficient in neuronal nitric oxide synthase, Science 265 (5180) (1994) 1883–1885.
[44] X. Li, et al., Chronic behavioral testing after focal ischemia in the mouse: functional recovery and the effects of gender, Exp. Neurol. 187 (1) (2004) 94–104.
[45] D. Mrdjen, et al., High-dimensional single-cell mapping of central nervous system immune cells reveals distinct myeloid subsets in health, aging, and disease, Immunity 48 (2) (2018), 380-395 e6.
[46] A. Grubman, et al., A single-cell atlas of entorhinal cortex from individuals with Alzheimer's disease reveals cell-type-specific gene expression regulation, Nat. Neurosci. 22 (12) (2019) 2087–2097.
[47] M. Olah, et al., Single cell RNA sequencing of human microglia uncovers a subset associated with Alzheimer's disease, Nat. Commun. 11 (1) (2020) 6129.
[48] K. Leng, et al., Molecular characterization of selectively vulnerable neurons in Alzheimer's disease, Nat. Neurosci. 24 (2) (2021) 276–287.
[49] A. Chamorro, et al., The immunology of acute stroke, Nat. Rev. Neurol. 8 (7) (2012) 401–410.
[50] A. Rayasam, et al., Contrasting roles of immune cells in tissue injury and repair in stroke: the dark and bright side of immunity in the brain, Neurochem. Int. 107 (2017) 104–116.
[51] S.G. Rhee, H.Z. Chae, K. Kim, Peroxiredoxins: a historical overview and speculative preview of novel mechanisms and emerging concepts in cell signaling, Free Radic. Biol. Med. 38 (12) (2005) 1543–1552.
[52] S.G. Rhee, et al., Peroxiredoxin functions as a peroxidase and a regulator and sensor of local peroxides, J. Biol. Chem. 287 (7) (2012) 4403–4410.
[53] J. He, et al., Oxidative stress, inflammation, and autophagy: potential targets of mesenchymal stem cells-based therapies in ischemic stroke, Front. Neurosci. 15 (2021) 641157.
[54] L. Garcia-Bonilla, C. Iadecola, Peroxiredoxin sets the brain on fire after stroke, Nat. Med. 18 (6) (2012) 858–859.
[55] M. Gelderblom, et al., Temporal and spatial dynamics of cerebral immune cell accumulation in stroke, Stroke 40 (5) (2009) 1849–1857.
[56] D. Berchtold, et al., Interaction of microglia with infiltrating immune cells in the different phases of stroke, Brain Pathol. 30 (6) (2020) 1208–1218.
[57] Z. Zhu, et al., Potential immunotherapeutic targets on myeloid cells for neurovascular repair after ischemic stroke, Front. Neurosci. 13 (2019) 758.
[58] L. Shi, et al., Treg cell-derived osteopontin promotes microglia-mediated white matter repair after ischemic stroke, Immunity 54 (7) (2021) 1527–1542 e8.
[59] Y. Zhang, A. Liesz, P. Li, Coming to the rescue: regulatory T cells for promoting recovery after ischemic stroke, Stroke 52 (12) (2021) e837–e841.
[60] Y. Yokosaki, et al., Distinct structural requirements for binding of the integrins alphavbeta6, alphavbeta3, alphavbeta5, alpha5beta1 and alpha9beta1 to osteopontin, Matrix Biol. 24 (6) (2005) 418–427.
[61] K.K. Jung, et al., Identification of CD63 as a tissue inhibitor of metalloproteinase-1 interacting cell surface protein, EMBO J. 25 (17) (2006) 3934–3942.
[62] A. Nimmerjahn, F. Kirchhoff, F. Helmchen, Resting microglial cells are highly dynamic surveillants of brain parenchyma in vivo, Science 308 (5726) (2005) 1314–1318.
[63] A.M. Planas, Role of immune cells migrating to the ischemic brain, Stroke 49 (9) (2018) 2261–2267.
[64] D.S.A. Simpson, P.L. Oliver, ROS generation in microglia: understanding oxidative stress and inflammation in neurodegenerative disease, Antioxidants 9 (8) (2020).
[65] A. Singh, et al., Oxidative stress: a key modulator in neurodegenerative diseases, Molecules 24 (8) (2019).
[66] R. Meller, et al., Neuroprotection by osteopontin in stroke, J. Cerebr. Blood Flow Metabol. 25 (2) (2005) 217–225.
[67] T.R. Hammond, et al., Single-cell RNA sequencing of microglia throughout the mouse lifespan and in the injured brain reveals complex cell-state changes, Immunity 50 (1) (2019) 253–271 e6.
[68] H. Ding, et al., Hepcidin is involved in iron regulation in the ischemic brain, PLoS One 6 (9) (2011), e25324..
[69] S.R. Rajendran, et al., Evaluation of serum ferritin as a prognostic marker in acute hemorrhagic stroke, J. Neurosci. Rural Pract. 11 (1) (2020) 72–77.
[70] B.B. Muhoberac, R. Vidal, Iron, ferritin, hereditary ferritinopathy, and neurodegeneration, Front. Neurosci. 13 (2019) 1195.